ORIGINAL PAPER

Auxetics and Other Systems of Anomalous Characteristics

physica status solidi b

www.pss-b.com

Negative In-Plane Poisson's Ratio for Single Layer Black Phosphorus: An Atomistic Simulation Study

*Duc Tam Ho, Viet Hung Ho, Harold S. Park, and Sung Youb Kim**

We utilized molecular statics (MS) simulations to investigate the auxeticity of single layer black phosphorus (SLBP). Our simulation results show that the SLBP has a negative in-plane Poisson's ratio in the zigzag direction when the applied strain along the armchair direction exceeds 0.018. We show that the interplay between bond stretching and bond rotating modes determines the in-plane Poisson's ratio behavior. While the bond stretching mode always tends to increase the in-plane auxeticity, the bond rotating mode might increase or decrease the in-plane auxeticity. Furthermore, we show that graphite also exhibits an in-plane negative Poisson's ratio at finite strains due to a similar mechanism.

1. Introduction

Auxetics are materials or structures that expand in the lateral direction when stretching in the longitudinal direction. There has been a wide range of structures with bulk form showing auxeticity based on different mechanisms including structures with re-entrant geometry,[1] theoretical models,[2,3] structures with rigid rotating units,[4] hinge structures[5,6] and elastic instability.[7] Some crystalline materials also exhibit auxeticity in some directions.[8–10] Recently, the investigation of auxetic property of nanoscale materials and structures using both numerical simulations and experiments have been received considerable attention.[11–14] The search for nanomaterials with negative Poisson's ratio (NPR) and the search for new mechanisms for NPR of nanomaterials have been significant.[15] Inspired by some existing mechanisms for bulk materials, some nanostructures involving defects or some specific engineered structures can show auxetic behavior such as patterned graphene structures based on rigid rotating unit model,[16] and wrinkled graphene structures based on de-wrinkling and unfolding mechanism.[17–19] In addition, auxeticity has been also found in nanoscale materials due to specific nanoscale physical properties that were not observed in materials and structures at macroscale. Surface effect in metal nanoplates and nanowires,[12,14] edge effect in graphene ribbons,[20] and puckered crystal structure of single layer black phosphorus (SLBP)[21] are some typical examples of the intrinsic mechanisms for auxeticity for nanoscale materials. Jiang et al. used molecular dynamics (MD) simulations with the second-generation Reactive Empirical Bond Order (REBO-II) potential[22] to show that pristine graphene can exhibit a NPR when the applied strain exceeds 0.06.[23] They have also shown that the interplay between the bond stretching and bond rotating modes are the origin for the auxeticity in the pristine graphene.

SLBP is a 2D material that is formed of parallel puckered double layers. Black phosphorus (BP) has been shown to have high hole mobility (the highest value up to 1000 $cm^2 V^{-1} s^{-1}$ for a thickness of 10 nm)[24–26] and its band gap can be tuned (from 1.51 eV for monolayer to 0.59 eV for a five layers).[27–29] BP is considered as an excellent thermoelectric material.[30–32] In addition, owing to its unique puckered structure, BP has highly anisotropic physical properties.[33–37] For example, few-layer BP has Young's modulus of 58.6 ± 11.7 and 27.2 ± 4.1 GPa in the zigzag (ZZ) and armchair (AC) directions, respectively, and the conductance anisotropy are found to be 63.7%. BP is used in many application fields such as batteries,[38–40] field effect transistors,[41–44] and nanoelectromechanical resonators.[45,46]

Inspired by the work of Jiang et al. on the NPR of pristine graphene,[23] we investigate the Poisson's ratios (PRs) of SLBP using molecular statics (MS) simulations with a Stillinger–Weber (SW) potential.[47] We present that the SLBP shows large anisotropic behavior, i.e., it can exhibit auxetic behavior in the ZZ direction when stretching the material in the AC direction at finite strains whereas the PR of the material along the AC direction when stretching the material along the ZZ direction is always positive. The auxetic behavior of SLBP is explained by the interplay between the bond stretching and the bond rotating modes. The simulation results show that at a small deformation $\varepsilon < 0.018$, the bond rotating mode is the dominant factor which leads to the positive PR. On the other hand, when $\varepsilon > 0.018$, the PR turns to a negative value, owing to the dominance of the bond stretching mode. In addition, we also show that the dominance of the bond stretching over the bond rotating at sufficient large strain is also the origin for auxeticity in graphite.

2. Simulation Methods

We performed MS simulations to predict the mechanical response of the SLPB by using the large-scale atomic/molecular

Dr. D. T. Ho†, V. H. Ho†, Prof. S. Y. Kim
Department of Mechanical Engineering, Ulsan National Institute of Science and Technology, Ulsan 44919, South Korea
E-mail: sykim@unist.ac.kr

Prof. H. S. Park
Department of Mechanical Engineering,
Boston University, Boston, MA 02215, USA

†These authors have contributed equally.

DOI: 10.1002/pssb.201700285

massively parallel simulator (LAMMPS).[48] We assigned the AC and ZZ directions as x- and y- directions, respectively. Periodic boundary conditions (PBCs) were applied along the x- and y-directions, while no PBC was applied in the out-of-plane direction. The SLBP model has the size of 43.61 Å × 66.29 Å, with 800 atoms. The configuration of the SLBP model with different views is shown in **Figure 1**a. As shown in Figure 1b, the geometry of the SLBP is characterized by the bond length r_1 which is the lengths of the bonds 1–2, 1–3, 4–5, and 4–6, the bond length r_2 which is the length of the bond 1–4, the angle α which is the angle between the bonds 1–2 and 1–3, (also the angle between the bonds 4–5 and 4–6), and the angle ψ which is the angle between the bond 1–4 and plane (456). In our simulations, the interaction between atoms was described by a SW potential.[47] For all simulations, the minimizations with the conjugate gradient method were terminated when the relative change of the energy of two adjacent iterations was less than 10^{-16}. For the simulations of graphite, the graphite model has the size of 12.3 Å × 21.3 Å × 13.4 Å, with 400 atoms and four layers of graphene. PBCs were applied along the x-, y-, and z-directions. The second-generation Reactive Empirical Bond Order (REBO-II) potential[22] was employed to describe the interaction between carbon atoms. In order to describe the van der Waals interaction between graphene layers, we used a Lennard–Jones potential with the energy parameter $\varepsilon = 0.0035$ eV, length parameter $\sigma = 3.354$ Å, and cut-off distance of 6.5 Å. With these parameters, the binding energy is calculated to be 51 meV/atom which is very close to the experimental result (52 ± 5 meV/atom).[49] Before applying loading, the structures were fully relaxed to attain their equilibrium states. After that, we applied strain with increments of 0.005 along the AC or ZZ direction. To model the uniaxial stress condition, only the stress component in the applied loading direction is non-zero whereas the simulation box is allowed to change so that other stress components are kept at zero. The PR is calculated as: $\nu = -\partial\varepsilon_t/\partial\varepsilon_a$, where ε_t and ε_a are the transverse and applied strain, respectively.

3. Results and Discussion

We begin by plotting the stress–strain curves of the SLBP under uniaxial stress conditions along the AC and ZZ directions in **Figure 2**. Due to the puckered structure, the mechanical properties are found to be highly anisotropic and nonlinear.[34] At the small strain, although both stress–strain curves are almost linear, the slopes of the curves are different from each other, i.e., the Young's moduli of the structure in the strain range of [0, 0.01] are 24.3 and 106 GPa along the AC and ZZ directions, respectively. Overall, the obtained Young's moduli are in excellent agreement with the results in some previous studies in which the same SW potential model was employed[50,51] (Table S1, Supporting Information). As the strain increases, the mechanical response becomes much more nonlinear. The stress reaches maximum at the strain of 0.3 and 0.16 for the cases of AC and ZZ loadings, respectively. These maximum stresses are the theoretical strengths of the SLBP along the AC and ZZ directions. It can be seen in Figure 2 that the theoretical strength for the AC direction is 7.8 GPa which is two times larger than that for the ZZ direction (3.9 GPa). For the case of AC loading condition, when the stress reaches the maximum, it then gradually decreases with the applied strain. It indicates that the material exhibits a negative linear compressibility in the loading direction because of elastic instability. It is noted that materials can be unstable at a stress smaller than the theoretical strength due to elastic instability[52] or phonon instability.[53] It is also noted that the negative linear compressibility can be obtained even in stable systems with internal constraints.[54,55] Finally, when the applied strain is sufficiently large, the stress shapely drops and becomes zero, indicating the brittle fracture of the material. The gradual decrease and the shape drop of the stress are also observed in the case of the ZZ loading condition, as shown in Figure 2. We also employed MD simulations at an extremely low temperature for the uniaxial tensile loading conditions along the AC and ZZ directions. The MD simulations results are in excellent agreement with the MS simulation when the applied strain is smaller than the critical strain at which the stress gets the maximum. Details of the comparison of the MS and MD simulation results can be seen in Fig. S1, Supporting Information.

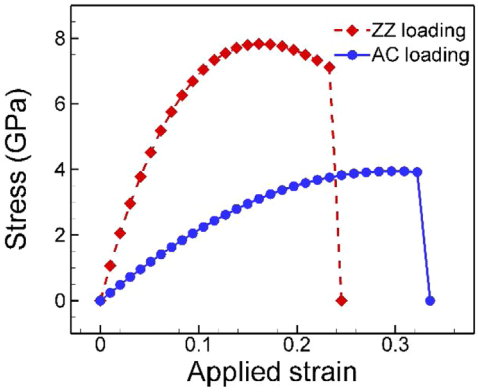

Figure 2. Mechanical responses of the SLBP under uniaxial tensile loading in the AC and ZZ directions. The results show the anisotropic mechanical properties of the SLBP.

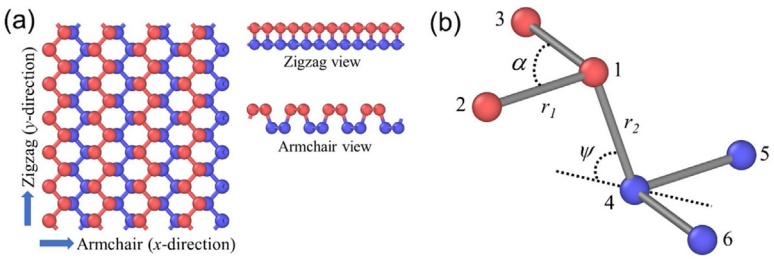

Figure 1. a) Structure of the SLBP at different views; and b) the characteristics geometry of the SLBP. Atoms are divided into top (red) and bottom group (blue).

We next examine the relation between transverse strains of the SLBP and the applied strain. It is confirmed once again that the SLBP is largely anisotropic even at small strains. In the case of

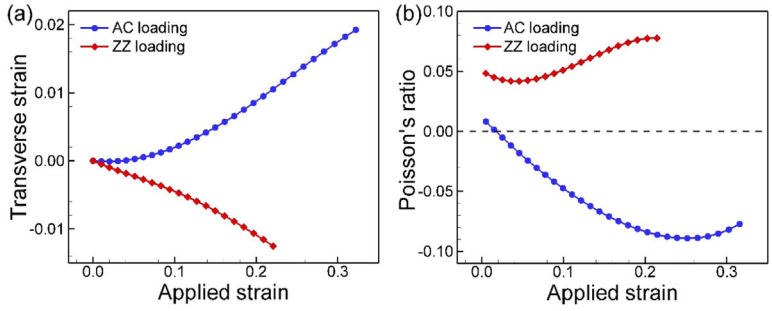

Figure 3. The changes of transverse strains (a) and the PRs (b) with applied strain of the SLBP under uniaxial tensile loading in the AC and ZZ directions. The NPR behavior is observed when the loading is applied in the AC direction.

stretching along the ZZ direction, the transverse strain monotonically decreases with the applied strain. The PR in this case is about 0.05 at the unstrained state and it changes slightly with the applied strain (**Figure 3**b). Meanwhile, the response of the transverse strain in the case of the AC loading is totally different. At small strain, the transverse strain slightly decreases with the applied strain. However, as the applied strain reaches 0.018, the transverse strain begins to increase. Thus, $\varepsilon = 0.018$ is the critical strain at which the PR of the SLBP turns from positive value to negative one. This critical strain is much smaller than the strain at which the stress gets its maximum ($\varepsilon = 0.3$) as mentioned before. Auxeticity at finite strain was also observed previously in metal nanoplates[12] as well as pristine graphene.[23] We note that the critical strain of the SLBP is much smaller than that of the pristine graphene (0.06), and that of the Al (001) nanoplate with the thickness of 2 nm (0.03).[12] Furthermore, our calculation shows that the smallest value of the PR in the SLBP is -0.09 whereas those of the pristine graphene and the Al (001) nanoplate are -0.05 and -2.0, respectively.

To explain the mechanism for the auxeticity in the SLBP, we also focus on the competition between the bond stretching and bond rotating modes suggested by Jiang et al.[23] As shown in Figure 1b, the geometry of the SLBP is characterized by the bond lengths r_1 and r_2, and the angles a and ψ. The length along the x-direction (AC direction) L_x and that along the y-direction (ZZ direction) L_y of the unit cell of the SLBP are:

$$L_x = 2\left(r_1 \cos\frac{a}{2} + r_2 \cos\psi\right) \quad (1)$$

$$L_y = 2r_1 \sin\frac{a}{2}. \quad (2)$$

Figure 4 shows the changes of the bond lengths and angles with the applied strain for the case of the AC loading. At undeformed configuration, the bond lengths are $r_1 = r_1{}^0 = 2.224$ Å and $r_2 = r_2{}^0 = 2.224$ Å, and the angles are $a = a^0 = 96.4^\circ$ and $\psi = \psi^0 = 71.6^\circ$. Under the loading, the bond lengths always increase with the applied strain. This elongation of the bond length is called bond stretching mode.[23] At small strains, r_1 and r_2 increase by almost the same amount; however, at larger strains, r_2 increases much faster than r_1 does. For the case of the angles, a slightly decreases until the applied strain reaches 0.18 but it then slightly increases, whereas ψ always decreases largely with the applied strain. The rotation of the bonds 1–2 and 1–3 around the atom 1 causes the change of a, and the rotation of the bond 1–4 around the atom 4 causes the change of ψ. We call the changes of the angles as bond rotating modes. For the case of stretching along the AC direction, the PR along the ZZ direction is determined by the change of the length L_y, which depends only on the bond length r_1 and the angle a, as shown in Eq. (2). Equation (2) indicates that if both r_1 and a increase/decrease, when stretching L_y increases/decreases, causing the expansion/contraction along the ZZ direction. We show in **Figure 5** the changes of r_1/r_1^0 and $\sin(a/2)/\sin(a^0/2)$ with applied strain. The composition of the two terms $(r_1/r_1^0)(\sin(a/2)/\sin(a^0/2))$ determines the mechanical property of the material at the current state. Since the bond length always increases with the applied strain, the term r_1/r_1^0 starts at 1 and linearly increases. On the other hand, the term $\sin(a/2)/\sin(a^0/2)$ is more non-linear and it largely decreases at small strain. As a result, the term $(r_1/r_1^0)(\sin(a/2)/\sin(a^0/2))$ is smaller than 1, as the applied strain is smaller than 0.018 (Figure 5). However, this term becomes larger than 1, as the applied strain is larger than 0.018. Consequently, the SLBP exhibits auxeticity as the applied strain exceeds 0.018, as shown in Figure 3b. It is worth noting for the case of AC loading that the angle a does not always decrease but it can instantaneously increase with the applied strain. Therefore, while the bond stretching mode of the SLBP always tends to enhance the auxeticity as in the case of graphene, the bond rotating mode causes a reduction or enhancement of the auxeticity which is different from the effect of bond rotating in graphene that only reduces the auxeticity of the material.

We now discuss on the PR of the SLBP along the AC direction when stretching the material along the ZZ direction. For the ZZ loading case, the PR behavior is determined by the change of the length L_x which not only depends on r_1 and a as in the case of AC stretching but also depends on r_2 and ψ, as

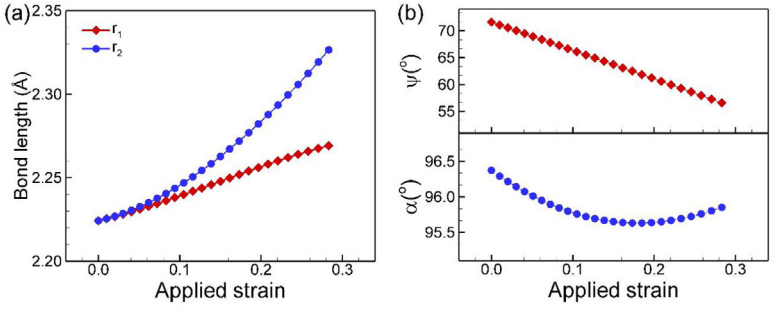

Figure 4. Displacements of atoms with applied strain when stretching the material along the AC direction. a) The changes of the bond lengths, and b) the changes of the angles.

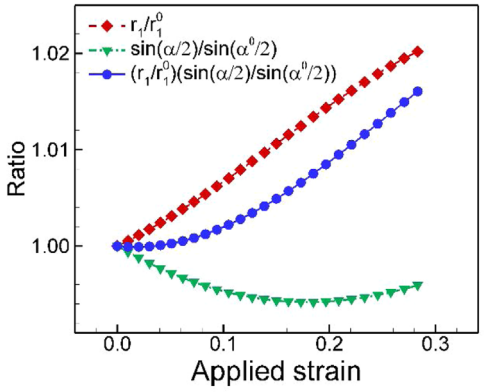

Figure 5. The interplay between the bond stretching and the bond rotating modes at different applied strains. The result shows that the bond stretching mode is more dominant than bond rotating mode as strain exceeds 0.018 so that the PR turns to negative at the critical strain of 0.018.

described in Eq. (1). As can be seen in Eq. (1), the increase of the bond lengths leads to the expansion, whereas the increase of the angles leads to the contraction of the structure in the x-direction. Under the ZZ loading, the bond length r_1 and the angle a linearly increase, the bond length r_2 seems to be unchanged, and the angle ψ linearly decreases with the applied strain. It indicates that the bond stretching of r_1 and the bond rotating ψ tend to enhance the auxeticity, the bond rotating a tends to reduce the auxeticity, and finally, r_2 does not play a role in changing the PR. The changes of the bond lengths and angles in the case of ZZ loading are different from those in the case of AC loading. When an amount of strain is applied along the AC direction, the bond 1–4 can rotate easily in the XZ-plane leading to the significant decrease of the angle ψ so that the change of r_1 and a are less significant. On the other hand, when an amount of strain is applied along the ZZ direction, the bond 1–4 does not rotate in the YZ-plane so that the bond 1–3 is significantly stretched and rotated. As can be seen clearly in **Figure 6**, r_1 increases about 7.2% and a does about 18% when the strain of 0.2 is applied to the material along the ZZ direction, whereas the corresponding values in the case of the AC loading are 1.5% and −0.8% for r_1 and a, respectively. Although r_1 is largely stretched and the angle ψ becomes smaller with applied strain resulting in an enhancement of auxeticity, the reduction of auxeticity by the increase of a is larger than the enhancement of auxeticity. That explains why the PR of the SLBP along the AC direction when stretching the material along the ZZ direction is always positive, as shown in Figure 3b.

We have discussed that the interplay of the two deformation modes, i.e., the bond stretching and the bond rotating determines the PR behavior of the SLBP. We now calculate the PRs of the graphite structure. **Figure 7**a shows the relation between the transverse strain and applied strain of the graphite. For the case of stretching along the ZZ direction, the calculated PR is still positive as the applied strain is smaller than 0.17. For the case of stretching along the AC direction, we note that there is a point around $\varepsilon_x = 0.06$ at which the transverse strain begins to increase with the applied strain. It indicates that graphite can exhibit a NPR along the ZZ direction when it is stretched along the AC direction with strains larger than 0.06 (Figure 7b). This strain is exactly the same as the critical strain for auxeticity in graphene in the work of Jiang et al.[23] As also shown in Figure 7b, the minimum PR is about −0.05 which is also the same as the minimum PR of the graphene in the work of Jiang et al.[23] It indicates that the effect of the weak van der Waals force between the layers on the PR in graphite is negligible. Moreover, it also indicates that the auxeticity in graphite is driven by the interplay between the bond stretching and bond rotating modes as in the case of SLBP as well as graphene.

It is worth noting that while in-plane auxeticity for SLBP is observed in this study using atomistic simulations with SW potential model, DFT calculation in a previous study showed that SLBP exhibits out-of-plane auxeticity, and that SLBP does not show a NPR in any in-plane direction.[21] In addition, graphene also shows auxetic behavior in the atomistic simulations with a Rebo-II potential, though it does not show any auxeticity in the DFT calculations.[56] Therefore, the use of empirical potentials in current work and the work by Jiang et al.[23] might not accurately capture the mechanical properties of actual SLBP and graphene. However, in this study, we do not aim to use atomistic simulations to determine precisely the mechanical property of actual SLBP. Rather, we focused on how and how much the auxeticity of covalently bonded materials is affected by bond stretching mode, bond rotating mode, and their interplay, and thus we employed SLBP structures described by the SW potential as a good example for this purpose. We showed that the interplay between bond stretching and bond rotating modes plays an important role in determining the PRs in covalently bonded materials. While the bond stretching mode tends to increase the auxeticity, the bond rotating mode might increase or decrease the auxeticity. Therefore, this study deals with two important issues in the study of auxeticity of nanoscale materials which are the search for new auxetic materials and the search for new mechanisms for auxeticity. It is

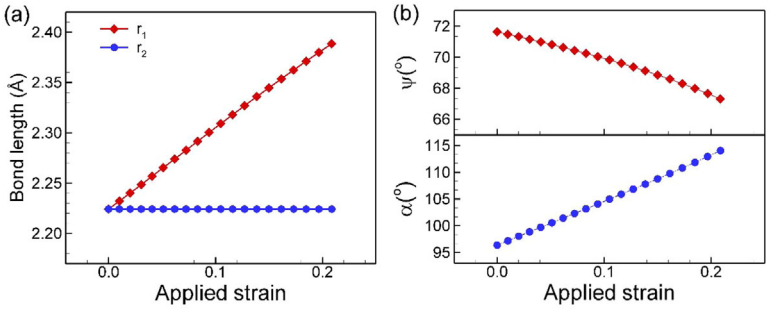

Figure 6. Displacements of atoms with the applied strain when stretching the material along the ZZ direction. a) The changes of the bond lengths, and b) the changes of the angles.

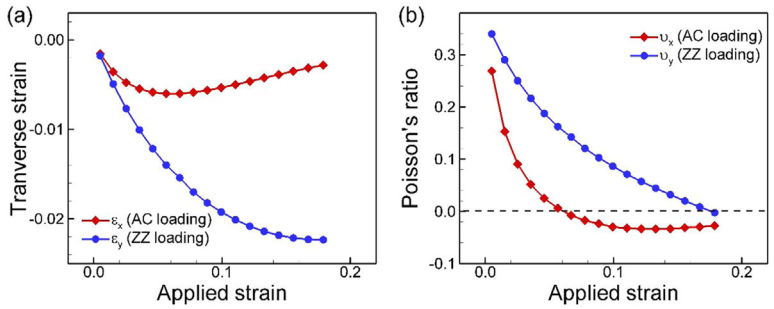

Figure 7. The changes of the transverse strains (a) and the PRs (b) with applied strain of the graphite under uniaxial tensile loading in the AC and ZZ directions. As in the case of the SLBP, auxeticity is only observed when stretching the material in the AC direction.

hoped that this mechanism can be used to explain auxeticity in other materials as in the case of semi-fluorinated graphene.[57] In addition, it is expected that the new mechanism can be exploited to design auxetic metamaterials at macroscale, which consist of similar structures of SLBP or graphene so that they are able to be governed by the stretching and rotating of their constituent parts, in near future.

4. Conclusion

In conclusion, we performed MS simulations with a SW potential to investigate the PR behavior of the SLBP. As stretching the material along the AC direction, we showed that the PR in the ZZ direction is positive at small strains and it turns to negative as the applied strain exceeds 0.018. The auxeticity is the result of the interplay between bond stretching and bond rotating modes. The bond stretching always tends to enhance the auxeticity, and the bond rotating can also enhance the auxeticity but it generally tends to reduce the auxetic behavior. We also found that graphite is able to exhibit auxeticity at finite strains with a similar mechanism. This study provides more examples for auxetic nanomaterials based on the bond stretching and bond rotating mechanisms at least in atomistic simulations with empirical potential models. It is hoped that the mechanism can be used to explain auxeticity for more materials, and that the mechanism can be exploited to design mechanical metamaterials with auxetic behavior in near future.

Supporting Information

Supporting Information is available from the Wiley Online Library or from the author.

Acknowledgements

We gratefully acknowledge the support from the ICT R&D Program (No R0190-15-2012) of Institute for Information communications Technology Promotion (IITP) and from the Mid-Career Researcher Support Program (Grant No. 2014R1A2A2A09052374) of the National Research Foundation (NRF), which are funded by the MSIP of Korea. We also acknowledge with gratitude the PLSI supercomputing resources of the KISTI and the UNIST Supercomputing Center. HSP acknowledges the support of the Mechanical Engineering department at Boston University.

Conflict of Interest

The authors declare no conflict of interest.

Keywords

atomistic simulations, black phosphorus, graphene, graphite, negative Poisson's ratio

Received: June 11, 2017
Revised: September 30, 2017
Published online: November 6, 2017

[1] R. Lakes, *Science* **1987**, *235*, 1038.
[2] K. W. Wojciechowski, *J. Phys. Math. Gen.* **2003**, *36*, 11765.
[3] K. W. Wojciechowski, *Phys. Lett. A* **1989**, *137*, 60.
[4] J. N. Grima, A. Alderson, K. E. Evans, *Phys. Status Solidi B* **2005**, *242*, 561.
[5] J. N. Grima, R. Jackson, A. Alderson, K. E. Evans, *Adv. Mater.* **2000**, *12*, 1912.
[6] J. N. Grima, R. Gatt, *Adv. Eng. Mater.* **2010**, *12*, 460.
[7] M. Taylor, L. Francesconi, M. Gerendás, A. Shanian, C. Carson, K. Bertoldi, *Adv. Mater.* **2014**, *26*, 2365.
[8] A. C. Brańka, D. M. Heyes, K. W. Wojciechowski, *Phys. Status Solidi B* **2009**, *246*, 2063.
[9] A. C. Brańka, D. M. Heyes, K. W. Wojciechowski, *Phys. Status Solidi B* **2011**, *248*, 96.
[10] D. T. Ho, S.-D. Park, S.-Y. Kwon, T.-S. Han, S. Y. Kim, *Phys. Status Solidi B* **2016**, *253*, 1288.
[11] Y. Du, J. Maassen, W. Wu, Z. Luo, X. Xu, P. D. Ye, *Nano Lett.* **2016**, *16*, 6701.
[12] D. T. Ho, S.-D. Park, S.-Y. Kwon, K. Park, S. Y. Kim, *Nature Commun.* **2014**, *5*, 3255.
[13] D. T. Ho, H. Kim, S.-Y. Kwon, S. Y. Kim, *Phys. Status Solidi B* **2015**, *252*, 1492.
[14] D. T. Ho, S.-Y. Kwon, S. Y. Kim, *Sci. Rep.* **2016**, *6*, 27560.
[15] J.-W. Jiang, S. Y. Kim, H. S. Park, *Appl. Phys. Rev.* **2016**, *3*, 041101.
[16] V. H. Ho, D. T. Ho, S.-Y. Kwon, S. Y. Kim, *Phys. Status Solidi B* **2016**, *253*, 1303.
[17] K. V. Zakharchenko, M. I. Katsnelson, A. Fasolino, *Phys. Rev. Lett.* **2009**, *102*, 046808.
[18] J. N. Grima, S. Winczewski, L. Mizzi, M. C. Grech, R. Cauchi, R. Gatt, D. Attard, K. W. Wojciechowski, J. Rybicki, *Adv. Mater.* **2015**, *27*, 1455.
[19] J.-W. Jiang, T. Chang, X. Guo, *Nanoscale* **2016**, *8*, 15948.
[20] J.-W. Jiang, H. S. Park, *Nano Lett.* **2016**, *16*, 2657.
[21] J.-W. Jiang, H. S. Park, *Nature Commun.* **2014**, *5*, 4727.
[22] D. W. Brenner, O. A. Shenderova, J. A. Harrison, S. J. Stuart, B. Ni, S. B. Sinnott, *J. Phys.: Condens. Matter* **2002**, *14*, 783.
[23] J.-W. Jiang, T. Chang, X. Guo, H. S. Park, *Nano Lett.* **2016**, *16*, 5286.
[24] L. Li, Y. Yu, G. J. Ye, Q. Ge, X. Ou, H. Wu, D. Feng, X. H. Chen, Y. Zhang, *Nature Nanotechnol.* **2014**, *9*, 372.
[25] J. Qiao, X. Kong, Z.-X. Hu, F. Yang, W. Ji, *Nature Commun.* **2014**, *5*, 4475.
[26] F. Xia, H. Wang, Y. Jia, *Nature Commun.* **2014**, *5*, 4458.
[27] V. Tran, R. Soklaski, Y. Liang, L. Yang, *Phys. Rev. B* **2014**, *89*, 235319.
[28] D. Çakır, H. Sahin, F. M. Peeters, *Phys. Rev. B* **2014**, *90*, 205421.
[29] J. Kim, S. S. Baik, S. H. Ryu, Y. Sohn, S. Park, B.-G. Park, J. Denlinger, Y. Yi, H. J. Choi, K. S. Kim, *Science* **2015**, *349*, 723.

[30] J. Zhang, H. J. Liu, L. Cheng, J. Wei, J. H. Liang, D. D. Fan, J. Shi, X. F. Tang, Q. J. Zhang, *Sci. Rep*. **2014**, *4*.
[31] E. Flores, J. R. Ares, A. Castellanos-Gomez, M. Barawi, I. J. Ferrer, C. Sánchez, *Appl. Phys. Lett*. **2015**, *106*, 022102.
[32] R. Fei, A. Faghaninia, R. Soklaski, J.-A. Yan, C. Lo, L. Yang, *Nano Lett*. **2014**, *14*, 6393.
[33] J. Tao, W. Shen, S. Wu, L. Liu, Z. Feng, C. Wang, C. Hu, P. Yao, H. Zhang, W. Pang, X. Duan, J. Liu, C. Zhou, D. Zhang, *ACS Nano* **2015**, *9*, 11362.
[34] J.-W. Jiang, H. S. Park, *J. Phys. D: Appl. Phys*. **2014**, *47*, 385304.
[35] H. Jang, J. D. Wood, C. R. Ryder, M. C. Hersam, D. G. Cahill, *Adv. Mater*. **2015**, *27*, 8017.
[36] X. Wang, A. M. Jones, K. L. Seyler, V. Tran, Y. Jia, H. Zhao, H. Wang, L. Yang, X. Xu, F. Xia, *Nature Nanotechnol*. **2015**, *10*, 517.
[37] R. Fei, L. Yang, *Nano Lett*. **2014**, *14*, 2884.
[38] L. Chen, G. Zhou, Z. Liu, X. Ma, J. Chen, Z. Zhang, X. Ma, F. Li, H.-M. Cheng, W. Ren, *Adv. Mater*. **2016**, *28*, 510.
[39] J. Sun, G. Zheng, H.-W. Lee, N. Liu, H. Wang, H. Yao, W. Yang, Y. Cui, *Nano Lett*. **2014**, *14*, 4573.
[40] L.-Q. Sun, M.-J. Li, K. Sun, S.-H. Yu, R.-S. Wang, H.-M. Xie, *J. Phys. Chem. C* **2012**, *116*, 14772.
[41] X. Liu, K.-W. Ang, W. Yu, J. He, X. Feng, Q. Liu, H. Jiang, D. Tang, J. Wen, Y. Lu, W. Liu, P. Cao, S. Han, J. Wu, W. Liu, X. Wang, D. Zhu, Z. He, *Sci. Rep*. **2016**, *6*, 24920.
[42] J. Kang, D. Jariwala, C. R. Ryder, S. A. Wells, Y. Choi, E. Hwang, J. H. Cho, T. J. Marks, M. C. Hersam, *Nano Lett*. **2016**, *16*, 2580.
[43] A. Avsar, I. J. Vera-Marun, J. Y. Tan, K. Watanabe, T. Taniguchi, A. H. Castro Neto, B. Özyilmaz, *ACS Nano* **2015**, *9*, 4138.
[44] M. Buscema, D. J. Groenendijk, S. I. Blanter, G. A. Steele, H. S. J. van der Zant, A. Castellanos-Gomez, *Nano Lett*. **2014**, *14*, 3347.
[45] C.-X. Wang, C. Zhang, J.-W. Jiang, H. S. Park, T. Rabczuk, *Nanoscale* **2016**, *8*, 901.
[46] Z. Wang, H. Jia, X. Zheng, R. Yang, Z. Wang, G. J. Ye, X. H. Chen, J. Shan, P. X. -L. Feng, *Nanoscale* **2014**, *7*, 877.
[47] J.-W. Jiang, *Nanotechnology* **2015**, *26*, 315706.
[48] S. Plimpton, *J. Comput. Phys*. **1995**, *117*, 1.
[49] R. Zacharia, H. Ulbricht, T. Hertel, *Phys. Rev. B* **2004**, *69*, 155406.
[50] Z. Yang, J. Zhao, N. Wei, *Appl. Phys. Lett*. **2015**, *107*, 023107.
[51] N. Liu, J. Hong, R. Pidaparti, X. Wang, *Nanoscale* **2016**, *8*, 5728.
[52] D. T. Ho, S.-D. Park, S.-Y. Kwon, T.-S. Han, S. Y. Kim, *EPL Europhys. Lett*. **2015**, *111*, 26005.
[53] D. M. Clatterbuck, C. R. Krenn, M. L. Cohen, J. W. Morris, *Phys. Rev. Lett*. **2003**, *91*, 135501.
[54] R. Lakes, K. W. Wojciechowski, *Phys. Status Solidi B* **2008**, *245*, 545.
[55] K. W. Wojciechowski, A. C. Brańka, *Mol. Phys. Rep*. **1994**, *6*, 71.
[56] F. Liu, P. Ming, J. Li, *Phys. Rev. B* **2007**, *76*, 064120.
[57] R. Qin, J. Zheng, W. Zhu, *Nanoscale* **2016**, *9*, 128.

